Draft version November 4, 2021
Typeset using LaTeX default style in AASTeX63

Multiband Detection of Repeating FRB 20180916B

Ketan R. Sand [1,2] Jakob Faber [1,2,3,4] Vishal Gajjar [4] Daniele Michilli [1,2,5,6] Bridget C Andersen [1,2]
Bhal Chandra Joshi [7] Sanjay Kudale [7] Maura Pilia [8] Bryan Brzycki [4] Tomas Cassanelli [9,10]
Steve Croft [11,12] Biprateep Dey [13] Hoang John [4] Calvin Leung [5,6] Ryan Mckinven [9,10]
Cherry Ng [10,11,12] Aaron B. Pearlman [1,2,14,*] Emily Petroff [1,2,15] Danny C. Price [16,4]
Andrew Siemion [11,17,12,18] Kendrick Smith [19] and Shriharsh P. Tendulkar [20,7]

[1] Department of Physics, McGill University, 3600 rue University, Montréal, QC H3A 2T8, Canada
[2] McGill Space Institute, McGill University, 3550 rue University, Montréal, QC H3A 2A7, Canada
[3] Department of Physics and Astronomy, Oberlin College, Oberlin, OH, 44074, U.S.A.
[4] Department of Astronomy, University of California, Berkeley, CA 94720, United States
[5] MIT Kavli Institute for Astrophysics and Space Research, Massachusetts Institute of Technology, 77 Massachusetts Ave, Cambridge, MA 02139, USA
[6] Department of Physics, Massachusetts Institute of Technology, 77 Massachusetts Ave, Cambridge, MA 02139, USA
[7] National Centre for Radio Astrophysics, Tata Institute of Fundamental Research, Post Bag 3, Ganeshkhind, Pune, 411007, India
[8] INAF - Osservatorio Astronomico di Cagliari - via della Scienza 5 - I-09047 Selargius, Italy
[9] David A. Dunlap Department of Astronomy & Astrophysics, University of Toronto, 50 St. George Street, Toronto, ON M5S 3H4, Canada
[10] Dunlap Institute for Astronomy & Astrophysics, University of Toronto, 50 St. George Street, Toronto, ON M5S 3H4, Canada
[11] Berkeley SETI Research Center, University of California, Berkeley, CA 94720, United States
[12] SETI Institute, Mountain View, CA, USA
[13] Department of Physics and Astronomy and PITT PACC, University of Pittsburgh, Pittsburgh, PA 15260, USA
[14] Division of Physics, Mathematics, and Astronomy, California Institute of Technology, Pasadena, CA 91125, USA
[15] Anton Pannekoek Institute for Astronomy, University of Amsterdam, Science Park 904, 1098 XH Amsterdam, The Netherlands
[16] International Centre for Radio Astronomy Research (ICRAR), Curtin University, Bentley WA 6102 Australia
[17] University of Manchester, Manchester, UK
[18] University of Malta, Malta
[19] Perimeter Institute for Theoretical Physics, 31 Caroline Street N, Waterloo, ON N25 2YL, Canada
[20] Department of Astronomy and Astrophysics, Tata Institute of Fundamental Research, Mumbai, 400005, India

(Received June 1, 2019; Revised January 10, 2019; Accepted November 4, 2021)

Submitted to AJ

ABSTRACT

We present a multiband study of FRB 20180916B, a repeating source with a 16.3 day periodicity. We report the detection of 4, 1 and 7 bursts from observations spanning 3 days using upgraded Giant Metrewave Radio Telescope (300-500 MHz), Canadian Hydrogen Intensity Mapping Experiment (400-800 MHz) and Green Bank Telescope (600-1000 MHz), respectively. We report the first-ever detection of the source in the 800-1000 MHz range along with one of the widest instantaneous bandwidth detection (200 MHz) at lower frequencies. We identify 30 μs wide structures in one of the bursts at 800 MHz, making it the lowest frequency detection of such structures for this FRB thus far. There is also a clear indication of high activity of the source at a higher frequency during earlier phases of the activity cycle. We identify a gradual decrease in the rotation measure over two years and no significant variations in the dispersion measure. We derive useful conclusions about progenitor scenarios, energy distribution, emission mechanisms, and variation of downward drift rate of emission with frequency. Our results reinforce that multiband observations are an effective approach to study repeaters and even one-off events to better understand their varying activity and spectral anomalies.

Corresponding author: Ketan Sand
ketan.sand@mail.mcgill.ca

Keywords: Radio Transient Sources – Fast Radio Bursts

1. INTRODUCTION

Fast Radio Bursts (FRBs) are millisecond duration pulses of unknown origin (see Cordes & Chatterjee 2019; Petroff et al. 2021; Chatterjee 2020 for review). Their anomalously high Dispersion Measure (DM) suggests an extragalactic origin, but an FRB detection by the Canadian Hydrogen Intensity Mapping Experiment/Fast Radio Bursts (CHIME/FRB; CHIME/FRB Collaboration et al. 2020) and Survey for Transient Astronomical Radio Emission 2 (STARE2; Bochenek et al. 2020) from magnetar SGR 1935+2154 has rekindled interests in Galactic FRB sources. Recent announcements by The CHIME/FRB Collaboration et al. (2021a) have led to a five fold increase in the source count with 607 published sources detected across 110 MHz (Pleunis et al. 2021; Pastor-Marazuela et al. 2021) to 8 GHz (Gajjar et al. 2018; Michilli et al. 2018). Earlier thought to be one-off events, sources with multiple bursts, called repeaters, have been found since the discovery of FRB 20121102A (Spitler et al. 2014). Presently, 21 repeaters are known, the majority of which have been discovered by CHIME/FRB (The CHIME/FRB Collaboration et al. 2019; Fonseca et al. 2020). Spectro-temporal studies of bursts from these sources have revealed interesting characteristic features, in particular, the downward drifting 'sad trombone' effect (Hessels et al. 2019) which has been observed in the dynamic spectra of many such events.

The repeater FRB 20180916B was discovered by CHIME/FRB (The CHIME/FRB Collaboration et al. 2019) and has been localized to spiral galaxy SDSS J015800.28+654253.0 at z = 0.0337 (Marcote et al. 2020). No persistent radio source has yet been discovered around the source. FRB 20180916B was found to be periodically active every 16.35 days (The CHIME/FRB Collaboration et al. 2020), with the period now refined to be 16.33$\pm$0.12 days with a 5.2 days activity window (Pleunis et al. 2021). It is the first FRB to be detected below 400 MHz by Sardinia Radio Telescope (SRT; Pilia et al. 2020), Green Bank Telescope (GBT; Chawla et al. 2020) and upgraded Giant Metrewave Radio Telescope (uGMRT; Sand et al. 2020) and the only FRB yet to be detected below 300 MHz by the Low Frequency Array (LOFAR; Pleunis et al. 2021; Pastor-Marazuela et al. 2021) in 110-188 MHz range. Interestingly even after more than 100 hours of observation spread across the entire 16.3 days period, using the Deep Space Network (DSN) 70 m telescope there were no detections from the source at 2.3 GHz and 8.4 GHz (Pearlman et al. 2020). Hence, so far the Effelesberg detections at 1.7 GHz by Marcote et al. (2020) are the highest frequency bursts reported from the source. This is dissimilar to what has been observed for FRB 20121102A which has been detected up to 8 GHz (Gajjar et al. 2018; Michilli et al. 2018).

The source is known to have a frequency dependence in its activity which was first observed by Aggarwal et al. (2020) in their Very Large Array (VLA) detection of the source at 1680 MHz at an earlier phase beyond the activity window determined by The CHIME/FRB Collaboration et al. (2020). This chromatic periodicity was then well established by Pastor-Marazuela et al. (2021) with their multiband observing campaign using Apertif (1370 MHz), LOFAR (150 MHz) and CHIME/FRB (600 MHz). They not only found increased activity at earlier phases at higher frequencies, but also proposed a narrower activity window as frequency increases. Pastor-Marazuela et al. (2021), however, did observe varying burst rates from the source even during expected 'peak' activity in the Apertif band and also conclude that the burst rate at LOFAR is higher than Apertif at a similar fluence threshold. This does make it crucial to undertake observations with wide bandwidth at different phases simultaneously to definitively estimate the burst rate variation with frequency as this will put quantitative limits on the activity and energy distribution which can help estimate some useful constraints on emission mechanism. Notably, repetition rate or even status as a repeater can be biased by observing frequency. FRB 20121102A and FRB 20180916B, are both good examples of this by showing no bursts at low (less than 400 MHz) and high frequencies (more than 1.7 GHz), respectively. Hence the simultaneous wideband study of repeaters or FRBs, in general, is the most efficient strategy to understand their enigmatic properties across large frequencies to eventually reveal possible progenitor scenarios.

The band-limited nature of repeaters makes it essential to have high-resolution simultaneous observations with a large bandwidth that can help detect variations in the spectro-temporal and even polarimetric structures of the bursts at different frequencies. The study of these contemporaneous frequency-dependent variations, as well as long term changes with time, are paramount in investigating the origins of FRBs. FRB 20121102A was one of the first repeater

* McGill Space Institute (MSI) Fellow.
* FRQNT Postdoctoral Fellow.

to be coherently corrected for dispersion, allowing unprecedented high-time resolution studies, revealing drifting bursts and an unusually high Rotation Measure (RM; Michilli et al. 2018; Gajjar et al. 2018; Hessels et al. 2019). Subsequent observations have shown a considerable decrease in the RM value with time (Hilmarsson et al. 2021). This variation is similar to what has been observed for Galactic centre Magnetar PSR J1745-2900 (Desvignes et al. 2018). On the other hand, FRB 20180916B has a nominal RM and has shown a gradual variation in RM value over two years timescale (Pleunis et al. 2021). These variations may be due to changes in the viewing geometry or the result of drastic variations in the circumburst environment facilitating magneto-ionic disparities. Interestingly, both of these FRBs show a flat Polarisation Position Angle (PPA) that can be indicative of emissions at higher altitudes due to relativistic shock (Beloborodov 2017; Metzger et al. 2019). Contrarily, observation of microstructures challenges this idea as in the case of FRB 20180916B such structures have been seen down to 2-3 μs (Nimmo et al. 2020) at 1700 MHz, hinting at emission much closer to the magnetosphere. Studying the evolution of such structures with frequency will aid in constraining the emission region and help understand the local environment. Another aspect of repeater burst morphology that remains a mystery is the 'sad trombone' effect, which describes a linear decrease in burst features with frequency and has been observed for FRB 20121102A and other repeaters, but it will be interesting to undertake a comparative study of this behaviour between frequencies.

Here, we present results from the observation campaign of FRB 20180916B using the uGMRT, GBT and CHIME/FRB. This paper includes a detailed analysis of uGMRT detections of FRB 20180916B (Sand et al. 2020) along with bursts during simultaneous GBT observations in the 600-1000 MHz range, we report the first detections of the source in the 800-1000 MHz range. We also report one CHIME/FRB detection within 0.04 activity phase of these detections [1]. In Sec. 2 we present details about the observations and instruments used. In Sec. 3 we provide the methodology that has gone in the analysis. In Sec. 4 we discuss the implications of our results; lastly, we provide concluding remarks in Sec. 5.

2. OBSERVATIONS

The source was observed using three telescope facilities, uGMRT, GBT and CHIME/FRB. These observations were undertaken on 2020 March 23 and 2020 March 24 (UTC) (see Table 1). One of the sessions for uGMRT was simultaneous with the GBT session (see Figure 1).The CHIME sessions selected are the transits of the source in the two days corresponding our observations.

Table 1. Table of observations and detections with columns listing telescope, frequency range for each session, start time of a session in UTC, duration of a given session in hours, and detected bursts for each session, respectively.

Telescope	Frequency Range (MHz)	Start Time in UTC	Duration of Observation (Hrs)	Bursts
GMRT	300 - 500	2020-03-23 06:31:19.566	0.67	
		2020-03-23 08:05:00.605	0.67	
		2020-03-23 08:05:00.605	0.67	
		2020-03-23 08:52:04.546	0.67	
		2020-03-23 09:38:44.327	0.67	GMRT A
		2020-03-23 10:25:18.740	0.67	GMRT B
		2020-03-24 06:17:57.000	0.67	
		2020-03-24 07:04:55.732	0.67	
		2020-03-24 07:52:23.832	0.67	GMRT C
		2020-03-24 08:40:05.354	0.67	
		2020-03-24 09:27:17.348	0.17	GMRT D
CHIME	400 - 800	2020-03-23 21:22:40	0.67	
		2020-03-24 21:26:40	0.67	CHIME A
GBT	600 - 1000	2020-03-24 06:46:26.440	1.67	GBT A-G

2.1. *Giant Metrewave Radio Telescope*

[1] This CHIME detection was previously published in Pleunis et al. (2021)

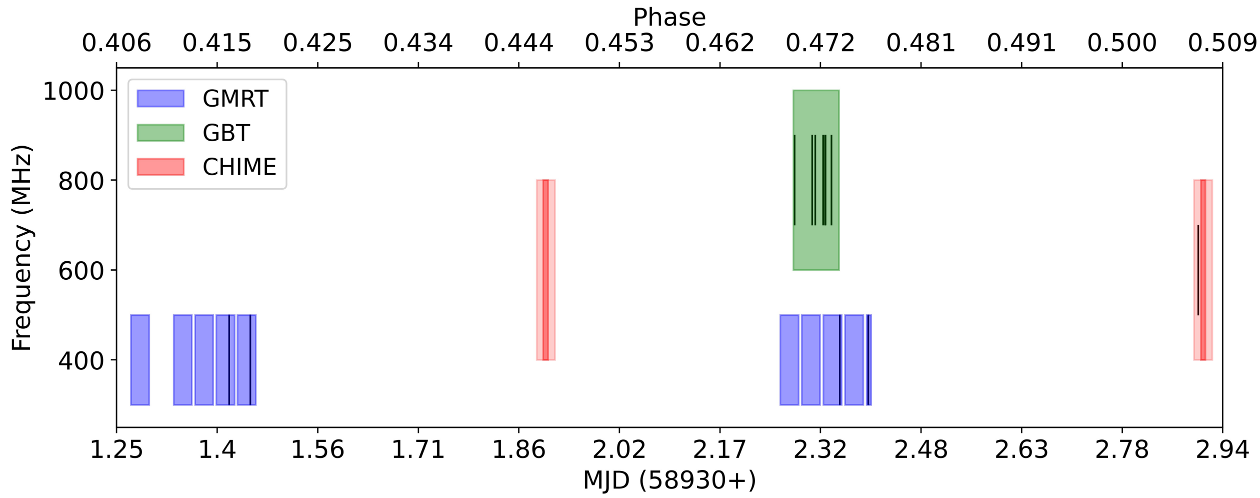

Figure 1. Observation epochs (in MJD and Phase) and frequency coverage for all telescopes. Bursts detected are shown with black solid lines for our semi-simultaneous multiband observations. The lighter shade in CHIME/FRB observations represents transit time in side lobes (end to end 40 mins), the darker region shows transit time through the beam FWHM ($\sim$ 10 mins). Phase has been calculated by folding at the period of 16.33 days with reference to MJD 58369.40 (Pleunis et al. 2021).

The uGMRT provides excellent capabilities for detecting FRBs at lower frequencies ($<$ 500 MHz) across a large instantaneous bandwidth of 200 MHz (Sand et al. 2020; Marthi et al. 2020; Pleunis et al. 2021). We observed FRB 20180916B during the activity window near the peak of its activity through a Target-of-opportunity (ToO) Director's Discretionary Time (DDT) proposal (Project code: DDTC 127). These observations were carried out at the Band 3 (250–500 MHz) of the uGMRT on 2020 March 23 and 2020 March 24 UTC (see Table 1). We formed tied array beams using 19 antennas which included 13 antennas from the central square and the first two antennas of each arm of the array. We used 3C48 for initial phasing and power equalization for all antennas. The uGMRT wide-band backend (GWB) is capable of recording four simultaneous beams (Reddy et al. 2017). We utilized one of the beams in voltage mode and coherently dedispersed incoming baseband voltages to the DM of 350 $\mathrm{pc\,cm^{-3}}$. We recorded 2048 dispersion corrected sub-bands with a temporal resolution of 81μsec. We also recorded another beam in a standard phased-array mode as a backup which was not utilized in these analyses. The high-time resolution filterbank data products were rid of any bright narrowband and broadband (zero DM) interference using `gptool` (Susobhanan et al. 2020) before converting them to `SIGPROC` (Lorimer 2011) formatted standard filterbank files.

The treated filterbank files were then searched for single pulse candidates using `SPANDAK`[2], which uses a GPU-based tool named `HEIMDALL` [3] (Barsdell et al. 2012) as the main kernel. This pipeline is similar to the one used by Gajjar et al. (2018) and Pilia et al. (2020) for detecting FRBs at 8 GHz and 300 MHz, respectively. To flag any remaining RFI, the `gptool` processed filterbank files were further checked for 'bad' channels using the `PRESTO`[4] `RFIFIND` algorithm. Then the data were searched using `HEIMDALL` for dedispersed pulses across a DM range of 0 to 500 $\mathrm{pc\,cm^{-3}}$. Candidates generated were then scrutinised by a Python based classification algorithm which crudely filtered out potential astrophysical candidates from noise spikes and RFI, taking into consideration maximum candidates per second (set to 4 in our case), S/N thresholds (6 sigma for GMRT), S/N-vs-DM distribution , and S/N-vs-boxcar width (maximum width set to 2048 time bins). The pipeline then extracted these shortlisted candidates from the original filterbank file, dedispersed them around their reported DMs and plotted dynamic spectra and burst profile across its time duration. The plots generated were then visually inspected. More details on the pipeline will be presented elsewhere. We identified 4 bursts, labeled as GMRT A-D, (see Figure 3) in the GMRT data after looking at more than 20,000 candidates generated by the pipeline. These bursts were then extracted as archive files at the native resolution of the filterbank files (frequency resolution $\sim$ 98 kHz, time resolution $\sim$ 81.92 μs) using `DSPSR` for further analysis.

[2] https://github.com/gajjarv/PulsarSearch

[3] https://sourceforge.net/p/heimdall-astro/wiki/Home/

[4] https://www.cv.nrao.edu/~sransom/presto/

One of the 40 mins scan from 2020 March 23 was corrupted due to interference and hence was not included in the further analysis (see Figure 1).

2.2. *Green Bank Telescope*

The observations with the GBT were conducted on 2020 March 24 (Table 1) across 680 – 920 MHz using the Breakthrough Listen digital backend (BLDB; MacMahon et al. 2018). The BLDB is a highly flexible state-of-the-art GPU-enabled 64-node compute cluster at the GBT. The BLDB is primarily deployed at the GBT to conduct one of the most comprehensive searches for intelligent life in the Universe (Worden et al. 2017; Gajjar et al. 2019; Isaacson et al. 2017). BLDB records 8-bit complex voltages with up to 12-GHz of instantaneous bandwidth across 64-compute nodes, with each node recording 187.5 MHz of bandwidth. We configured it to record across 614 – 989 MHz (375 MHz of total bandwidth), covering the 680 – 920 MHz receiver bandwidth, utilizing two compute nodes. These observations were done in simultaneity with one of the uGMRT epochs (see Figure 1). We recorded complex voltages into the Green Bank ultimate pulsar processing instrument (GUPPI) format with the native sampling time of 341 ns with 128 polyphase coarse channels (see Lebofsky et al. 2019). These raw voltages were converted to total intensity `SIGPROC` filterbank files with a spectral and temporal resolution of $\sim$350 kHz and 349 μsec, respectively for searching. A similar search for FRBs was done here as described for GMRT bursts using `SPANDAK`, with a few exceptions. Firstly, we did not treat the files for RFI before converting them to `SIGPROC`-filterbank files. Secondly, we performed a sub-banded search (dividing the band into 8 sub-bands) to identify low-intensity and narrow band (also referred to as 'smudgy') bursts. This search (above 6 sigma) revealed 7 real candidates (GBT A-G, figure 3) after an initial visual examination of around 5000 candidates, followed by a cross-referencing of candidates detected in individual sub-bands to pick out coincident signals that extended beyond a single sub-band. Once we had identified all bursts in the data, we then extracted their raw voltages and coherently dedispersed them around a fiducial DM of 349 $\mathrm{pc\,cm^{-3}}$ using `DSPSR`, to produce archive files of desired time and frequency resolutions depending on the analysis involved. After a detection of a bursts at the GBT, we carefully again re-examined uGMRT data around the same epoch (correcting for dispersion delay). Figure 2 shows a clear detection of a burst at GBT while at the same instant, uGMRT does not show any indication of any dispersed burst. This confirms that, similar to FRB 20121102A (Law et al. 2017), burst from FRB 20180916B are highly spectrally limited.

2.3. *CHIME/FRB*

CHIME is a radio interferometer observing in the 400–800 MHz range. The CHIME/FRB backend (CHIME/FRB Collaboration et al. 2018) provides the capability of detecting and studying the FRB population (The CHIME/FRB Collaboration et al. 2021b). With its real-time pipeline, CHIME/FRB continuously monitors the large ($\sim$ 200 square degrees) field of view of the telescope for impulsive, dispersed signals. RFI is automatically discarded with a dedicated machine-learning algorithm and a few seconds of total intensity data are stored around signals of interest for further analysis (The CHIME/FRB Collaboration et al. 2021b). These data have a time resolution of 0.98 ms and a frequency resolution of 24.4 kHz.

One burst (Figure 3, bottom right) from FRB 20180916B was detected by the CHIME/FRB within one day of the detections from the GMRT and GBT summarised in Table 2. We calculated its peak flux and fluence by using steady sources as calibrators following previous work presented by CHIME/FRB Collaboration et al. (2019) and The CHIME/FRB Collaboration et al. (2021b).

3. ANALYSIS

The analysis presented here is used in the characterization of GMRT and GBT bursts. The details regarding estimation of properties for the CHIME/FRB burst has been presented in Pleunis et al. (2021).

3.1. *Burst Properties, Scattering, and Micro-structures*

Both the GMRT and GBT bursts exhibit complex morphology. As seen in Figure 3, GMRT A shows a downward drifting substructure, with GMRT B displaying what seems to be a scattering tail but can also be some unresolved structures. GBT B and GBT E both show drift in the spectra, with GBT F exhibiting microstructures (Figure 4). These structures will be hindered if we dedisperse as per S/N, hence to estimate the structure maximising DM we used the `DM phase` (Seymour et al. 2019) package[5]. This algorithm maximises the coherent power of the bursts. To

[5] https://github.com/danielemichilli/DM_phase

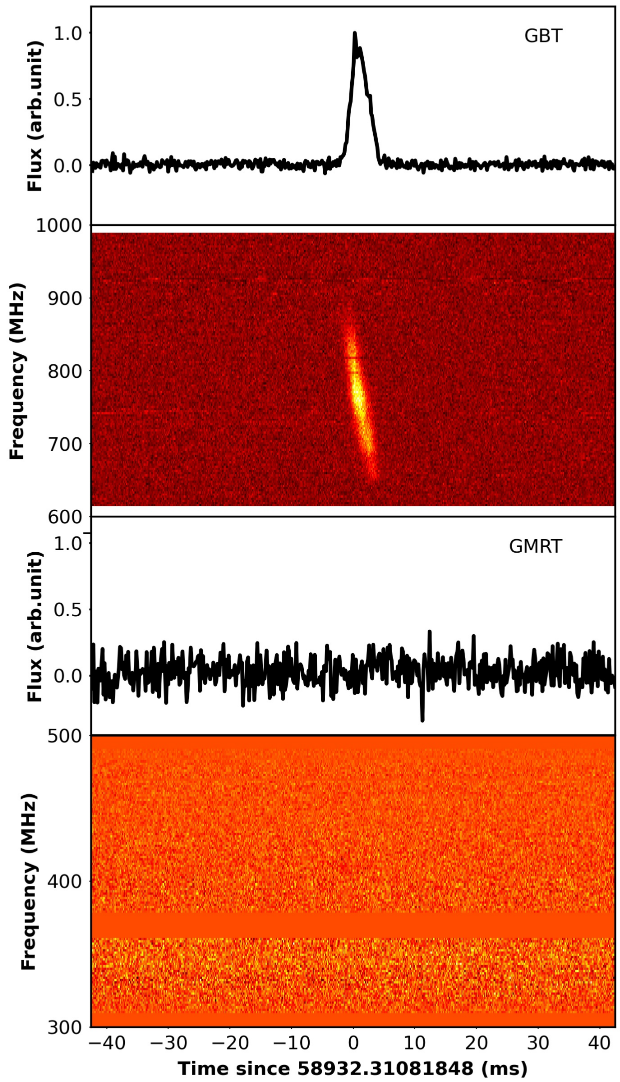

Figure 2. Simultaneous GBT and GMRT observations of a burst (GBT B) only detected at GBT. The top panels in both plots show integrated and dedispersed time-series while the second panels in both plots show dedispersed dynamic spectra at the DM of 348.8 $\mathrm{pc\,cm^{-3}}$. We clearly see band limited nature of these bursts and confirm that the burst energy is within our observed frequency range.

estimate the best DM each burst was dedispersed around a trial DM (348.7 $\mathrm{pc\,cm^{-3}}$), the `DM Phase` package then tested from -6 to +6 values around the trial DM with steps of 0.01 to ascertain the structure maximising DM. We got DM values for all bursts within 348.6-350.2, which is consistent with the DM reported for this FRB. For the GBT E, the highest S/N burst in our dataset, we found the structure maximising DM of 348.9±0.1. We then dedispersed all other bursts around this DM range (348.8-349.0 $\mathrm{pc\,cm^{-3}}$) and after a visual examination found that the DM of 348.8 $\mathrm{pc\,cm^{-3}}$ seems to maximise structures for all the bursts in our dataset (see Figure 3). Thus, this DM was then used in all the analysis reported here.

To estimate width and scattering, we used `bilby`[6], a Bayesian inference library, to perform a nested sampling fit of multiple exponentially-modified gaussian profiles—one for each sub-burst. The division of bursts into sub-burst was approximated based on the appearance of intensity variations in each burst profile. The sub-burst widths were summed over to get the total width of the burst. We obtain scattering timescales from an exponential fit to the

[6] https://lscsoft.docs.ligo.org/bilby/index.html

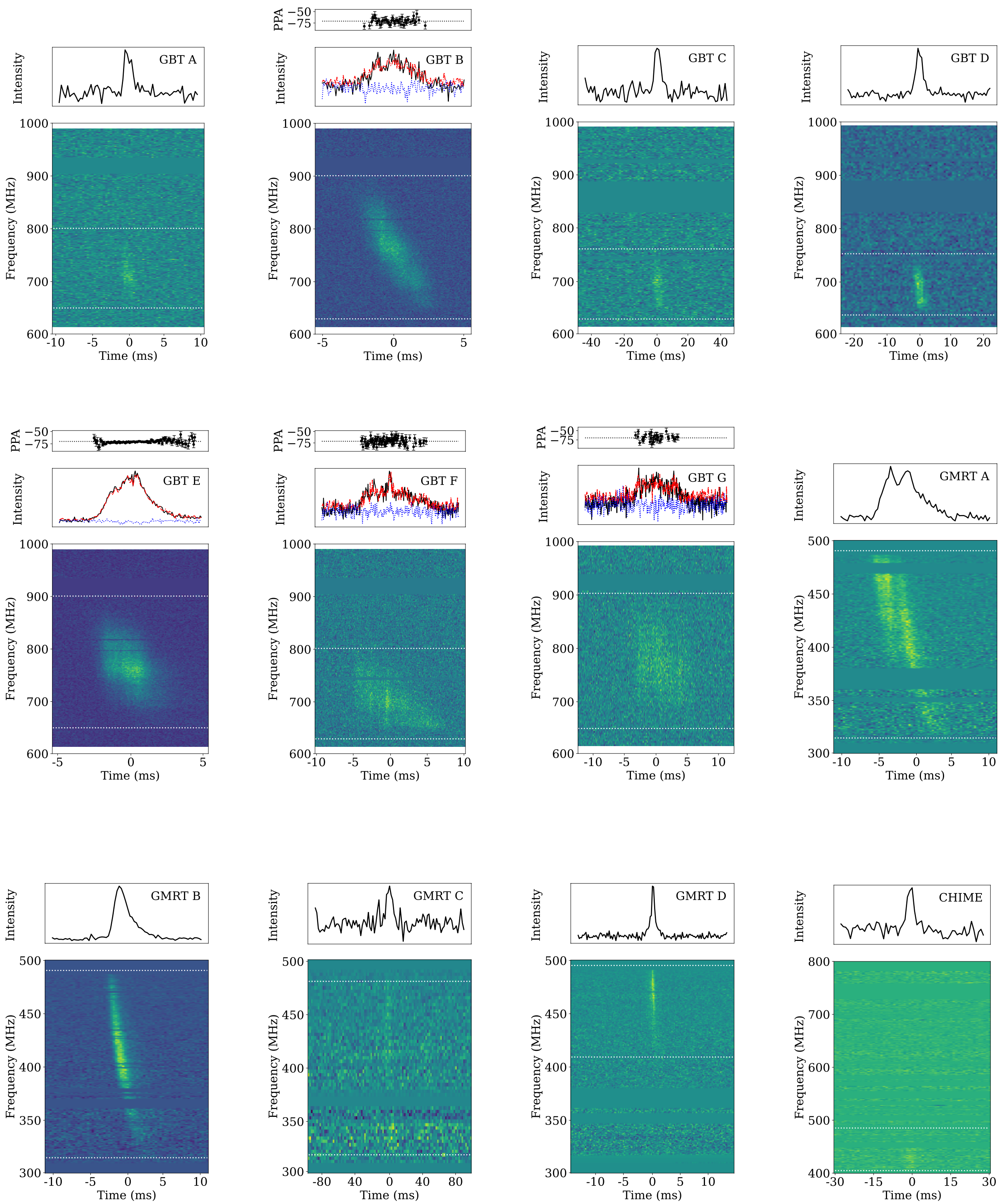

Figure 3. Waterfall plots of all 12 reported bursts. The top panel shows the integrated profile with bottom panel showing flux as function of time and frequency. Each burst has been dedispersed to a DM of 348.8 $\mathrm{pc\,cm^{-3}}$, the structure maximising DM for the highest S/N burst in our dataset (GBT E, see section 3.1), except bursts GBT D (349.8 $\mathrm{pc\,cm^{-3}}$), GMRT C (350 $\mathrm{pc\,cm^{-3}}$) and CHIME (349.5 $\mathrm{pc\,cm^{-3}}$) which were too weak to be seen around this DM. For GBT bursts B, E, F, and G, circular (blue) and linear (red) polarization and PPA referenced to infinite frequency are plotted against the respective timeseries.

Table 2. Burst properties of detected bursts from FRB 20180916B. Columns list arrival MJDs (barycentered and referenced to infinite frequency), peak S/N, fractional bandwidth of burst emission, measure burst width, peak flux, fluence, and temporal resolution of underlying data products used for these measurements, respectively.

Burst	MJD	Peak S/N	$\Delta\nu$	Width	Peak Flux	Fluence	$t_{\rm peak}$
	(58932+)	Full/$\Delta\nu$	(MHz)	(ms)	Full/$\Delta\nu$ (Jy)	Full/$\Delta\nu$ (Jy ms)	(ms)
GBT A	0.2827216	7.85/18.12	46	2.8(1.5)	0.29(2)/1.51(9)	0.35(21)/1.8(1.1)	0.33
GBT B	0.3093268	37.17/46.05	179	3.13(51)	2.04(25)/3.19(39)	2.72(77)/4.2(1.2)	0.16
GBT C	0.3141119	6.16/11.74	81	7.0(1.6)	0.12(1)/0.39(1)	0.35(8)/1.19(27)	1.3
GBT D	0.3260644	8.51/18.15	86	2.4(1.5)	0.23(1)/0.95(3)	0.24(15)/0.98(62)	0.65
GBT E	0.3291835	80.22/97.75	146	3.28(61)	4.39(55)/7.03(87)	6.1(1.9)/9.8(3.1)	0.16
GBT F	0.3297834	14.33/24.84	118	10.3(2.6)	0.54(3)/1.47(9)	2.41(75)/6.5(2.1)	0.33
GBT G	0.3388846	13.69/17.99	177	8.2(1.9)	0.52(3)/0.95(5)	1.83(53)/3.33(97)	0.33
GMRT C	0.3516781	9.85/9.85	<200	< 8.4(2.3)	0.43(1)/0.43(1)	1.55(45)/1.55(45)	1.9
GMRT D	0.3952298	20.48/46.56	74	6.5(1.8)	1.29(3)/4.98(12)	3.6(1.1)/13.8(4.2)	0.8
CHIME[a]	0.8983427	13.0	< 50	3.1(3)	> 0.4(2)	> 1.6(6)	0.98
	MJD (58931+)						
GMRT A	0.4200371	24.58/25.65	171	5.82(73)	2.53(15)/2.85(17)	6.2(1.1)/7.1(1.2)	0.33
GMRT B	0.4523516	67.39/67.39	>200	2.46(47)	6.92(42)/6.92(42)	7.2(1.9)/7.2(1.9)	0.33

[a] Properties estimated using CHIME pipelines as described in Pleunis et al. (2021)

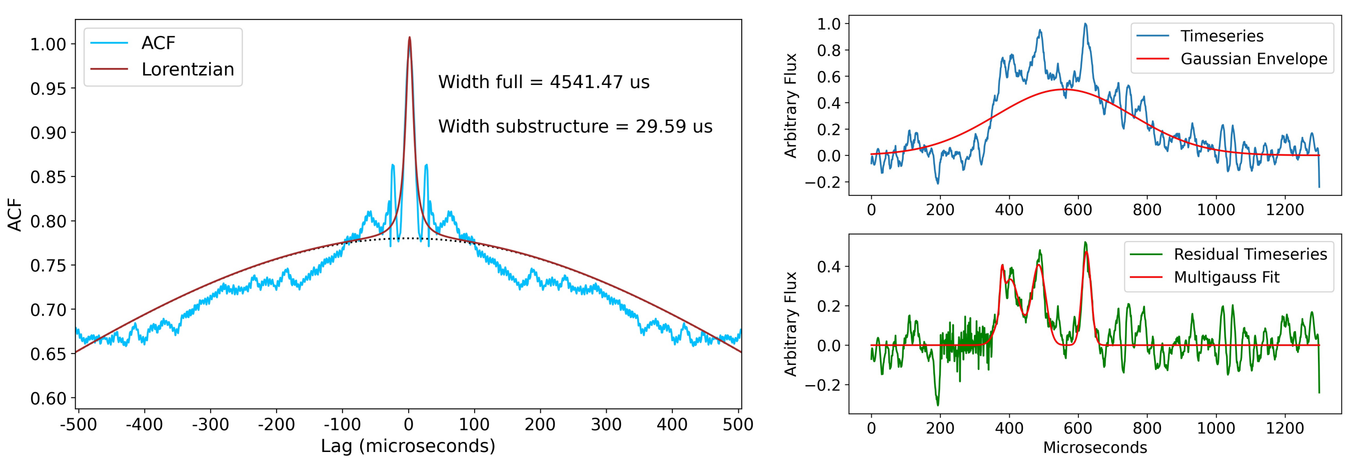

(a) (b)

Figure 4. Microstructure analysis for GBT F burst. (a) Time series autocorrelation of GBT F to study mircrostructure. The width of the structure is estimated to be 30 μs using a Lorentzian fit. (b) The 4 μs timeseries of the same burst with envelope subtracted residual showing clear structures.

latest (right-most) sub-burst in the profile. We find varying scattering estimates for GMRT and GBT bursts (Table 3). Only those bursts were selected which showed an exponential tail which can possibly be attributed to scattering. Our scattering time-scale measurements for GMRT bursts, particularly GMRT B with ~ 1.7 ms which shows a clear exponential tail, is in agreement with what has been observed for the source around similar frequencies by Chawla et al. (2020).

FRB 20180916B has already been reported to exhibit sub-microsecond structure at 1.4 GHz (Nimmo et al. 2020). We also performed auto-correlation (ACF) analysis to investigate microsecond structure in our bursts detected from the GBT at 800 MHz; where we had retained baseband voltages. Unfortunately, such a study was not possible to perform for bursts detected from GMRT due to insufficient S/N and poor temporal resolution of our data products.

In order to look for microstructures, we again coherently dedisperse baseband voltages and produce higher temporal resolution data products of 4 μs. We performed an ACF on the dedispersed and frequency-averaged time series for one the bursts, GBT F, which was already showing noticeable sub-structures (see Figure 3). As shown in Figure 4a, the ACF showed a significant peak. The measured widths of the ACF from an Lorentzian fit is around 30 μsec. Such micro-structures are readily seen in Figures 4b, once a Gaussian envelope of the overall burst shape is removed.

To estimate the peak flux for our detected bursts, we used the radiometer equation (Lorimer & Kramer 2004) which can be expressed as,

$$S_{\rm peak} = \beta \frac{(S/N)_{\rm peak} T_{\rm sys}}{G\sqrt{n_p \Delta\nu t_{\rm peak}}}. \tag{1}$$

Here, $T_{\rm sys}$ is the system temperature (receiver + sky), $\Delta\nu$ is the bandwidth, G is the gain of the telescope, β is the digitisation factor (quantum efficiency), $n_{\rm p}$ is the number of polarisation channels and $t_{\rm peak}$ is the temporal resolution of the burst profile. The $(S/N)_{\rm peak}$ was calculated after normalizing time series by subtracting the mean of off-pulse region from on-pulse region, where the on-pulse region was defined by visually inspecting burst profile for each burst. For GBT [7], $\beta \sim 1$, $T_{\rm sys} = 38\,{\rm K}(29\,{\rm K} + 9\,{\rm K})$, G = 2 K/Jy, $\Delta\nu$ = 375 MHz and $n_{\rm p} = 2$. In case of GMRT, an additional antenna term $\sqrt{\delta N_{\rm ant}(N_{\rm ant} - 1)}$ was multiplied in the denominator, where $N_{\rm ant} = 19$ corresponds to number of antennas employed to create a phased array and δ accounts for the linear degradation of phasing that will lead to loss of sensitivity. For example, by carefully monitoring the phasing at the beginning and at the end of a single 40-min long scan, we noticed a decrease in δ from 0.8 to 0.65, which we assumed to follow a linear trend to affect flux estimates for different bursts detected across the length of a scan. Other values[8] were taken to be - T_{sys} = 218 K (165 K + 53 K), $n_p = 2$, $G = 0.38 K/Jy$, $\Delta\nu$ = 200 MHz. The sky temperature in case of GMRT (53 K) and GBT (9 K) were estimated using 408 MHz sky temperature map from Haslam et al. (1982) and using spectral index of -2.55 (Remazeilles et al. 2015), extending to central frequencies of 400 MHz and 800 MHz, respectively. As seen in Figure 3, many bursts exhibit spectrally limited emission, thus, we measured peak fluxes and fluences from full bandwidth and fractional bandwidth for each burst. This fractional bandwidth was determined by a Gaussian fit to each burst spectrum (Zhang et al. 2018). The fluences for full and fractional bandwidth were calculated by summing over full width half maximum temporal width and averaging over full and fractional bandwidth, respectively. Table 2 summarises these properties for reported bursts from GMRT, GBT, and CHIME.

3.2. *Drift-rate estimation*

One of the most notable morphological features present in repeating FRBs is sub-pulse drifting (also known as the "sad trombone" effect). Drifting appears as the downward progression of the observed frequency of the sub-pulses comprising a burst as a function of time. This can appear in bursts that are cohesive in time (exhibiting no features between which the power drops to the noise level)—i.e., the majority of bursts in this data set—as well as bursts that are made up of discrete sub-bursts, such as GMRT A. One method that has been used thus far to calculate drift rates in FRBs involves transforming the dynamic spectrum to spectro-temporal lag space by taking its 2D auto-correlation function, followed by using MC sampling to fit an ellipse to the delay spectrum, and finally deriving the drift rate from the tilt of its semi-major axis (Hessels et al. 2019; Gourdji et al. 2019). Here we present the results achieved by using a slightly different method that, to the best of our knowledge, has not been used for measuring drift rates in the past.

The method implemented here is achieved through elliptical isophote analysis using the a package within `Astropy` called `photutils` which, similar to the standard method, is performed on the 2D auto-correlation of the dynamic spectrum. The isophotometry algorithm iteratively samples pixels along trial ellipses of varying ellipticity and position angle in the ACF for a given semi-major axis length, hoping to identify pixels with similar intensity which indicate a good description of (or fit to) an isophote. We have chosen to avoid sampling for small semi-major axis values due to significantly higher intensities in bins that occupy the center of the ACF. As seen in Figure 5a, the elliptical isophotes were sampled and plotted to the FWHM of the ACF for burst GBT B. Figure 5b shows the original waterfall plot, over which a dotted white line has been plotted with the averaged slope of all sampled isophotes in the ACF. The drifting estimates vary for GMRT and GBT bursts (Table 3), GMRT A has a clear sub-burst drift of around -13.6 MHz ms^{-1} which is less than the drift observed for brighter GBT bursts in particular GBT B with drift of around -36

[7] https://science.nrao.edu/facilities/gbt/proposing/GBTpg.pdf

[8] http://indrayani.ncra.tifr.res.in/~secr-ops/sch/c41webfiles/gtac_41_status_doc.pdf

MHz ms^{-1}. This linear variation with frequency (see Figure 7a) is similar to what has been observed for repeaters notably FRB 20121102A which showed higher drift rate in its 8 GHz detections (Gajjar et al. 2018) compared to its L-band detections (Hessels et al. 2019).

3.3. *Polarimetry*

We carried out measurements of the polarization properties of the GBT bursts as we only recorded total intensity for the GMRT bursts. To measure polarization, we first extracted the baseband raw voltage data for four GBT bursts (GBT B, GBT E, GBT F and GBT G) with sufficiently high S/N values and coherently dedispered it at the previously measured DM of 348.8 pc cm^{-3}. These products were stored in full-Stokes `PSRFITS` format at resolutions of 40 μsec and 97.66 kHz for all four bursts.

The remaining bursts detected from the GBT did not offer sufficient S/N to reliably extract any polarisation information. During the observations, a noise diode-scan was performed at the beginning of the observing run. This noise diode scan on the source was used for polarization calibration. We used the `PSRCHIVE`'s `pac` routine to calibrate our `PSRFITS` file for each burst.

To measure the RM of each burst, we utilized two algorithms in tandem, both of which are implemented by the `rmfit`[9] tool within `PSRCHIVE`. The first is a brute-force calculation of fractional linear polarization for a series of trial RM values. The value achieved with this method is used as an initial guess for the second algorithm, which performs an iterative refinement of the differential PPA. This involves dividing the band in two and calculating the weighted differential polarization angle between each half. For the latter method, as long as the weighted differential PPA is greater than its uncertainty, the data are iteratively corrected for the corresponding RM trial value until the weighted differential PPA is less than its uncertainty. We also measured the RM contribution from ionosphere using `ionFR`[10] (Sotomayor-Beltran et al. 2013) which was found to be + 0.1 rad m^{-2} around the arrival time of all the GBT bursts. Table 3 reports the RM values after correcting for this ionospheric contribution. The RM values we obtain are slightly less than the values first measured for this source (The CHIME/FRB Collaboration et al. 2019), but remain consistent with the most recent measurements (Nimmo et al. 2020) within an uncertainty of 1σ.

The effect of Faraday rotation was corrected to the measured RM values of each individual burst, all of which are recorded in Table 3, with an average value of -117.6 rad m^{-2}. The correction reveals nearly 100% linear polarization and stable PPA curves across pulse phase, as shown in Figure 3. We also noticed flat PPA during the saddle emission between sub-bursts, which confirms findings recently reported by Nimmo et al. (2020). The linear polarization plotted over bursts GBT B, E, F, and G adheres to the complex sub-structures of each burst—confirming that these sub-structures are indeed physical.

Table 3. Spectro-temporal and polarization properties for selected bursts detected from GBT and GMRT. The columns from left to right reports, burst name, measured RM, mean PPA at infinite frequency in barycentric reference frame, standard deviation on the measured PPA, scattering timescale, measured DISS bandwidth, and drift rate of downward drifting emission. The RM reported here is corrected for ionospheric contribution of + 0.1 rad m^{-2} (see Section 3.3)

Burst	$\mathrm{RM_{obs}}$ (rad m^{-2})	$\mathrm{PPA}_\infty^{\mathrm{mean}}$(deg)	$\Delta\mathrm{PPA}_\infty$(deg)	τ_s (ms)	$\Delta\nu_{\mathrm{DISS}}$ (kHz)	Drift Rate (MHz/ms)
GBT B	-117.5(5)	-71.4(8)	6	...	2.6(6)	-35.7(8)
GBT E	-117.7(2)	-71.30(2)	4	1.16(31)	4.2(2)	-18.6(8)
GBT F	-117.4(9)	-71.4(4)	7	...	...	-8(1)
GBT G	-117.2(9)	-69(1)	8	...	...	-10(2)
GMRT A	...	...	...	2.51(37)	...	-13.6(6)
GMRT B	...	...	...	1.67(47)	...	...

3.4. *Scintillation studies*

We investigated the scintillation (decorrelation) bandwidth for GBT B and E. We required a high frequency resolution to resolve the bandwidth predicted by the NE2001 Galactic electron density model (Cordes & Lazio 2002) –

[9] http://psrchive.sourceforge.net/manuals/rmfit/

[10] https://github.com/csobey/ionFR

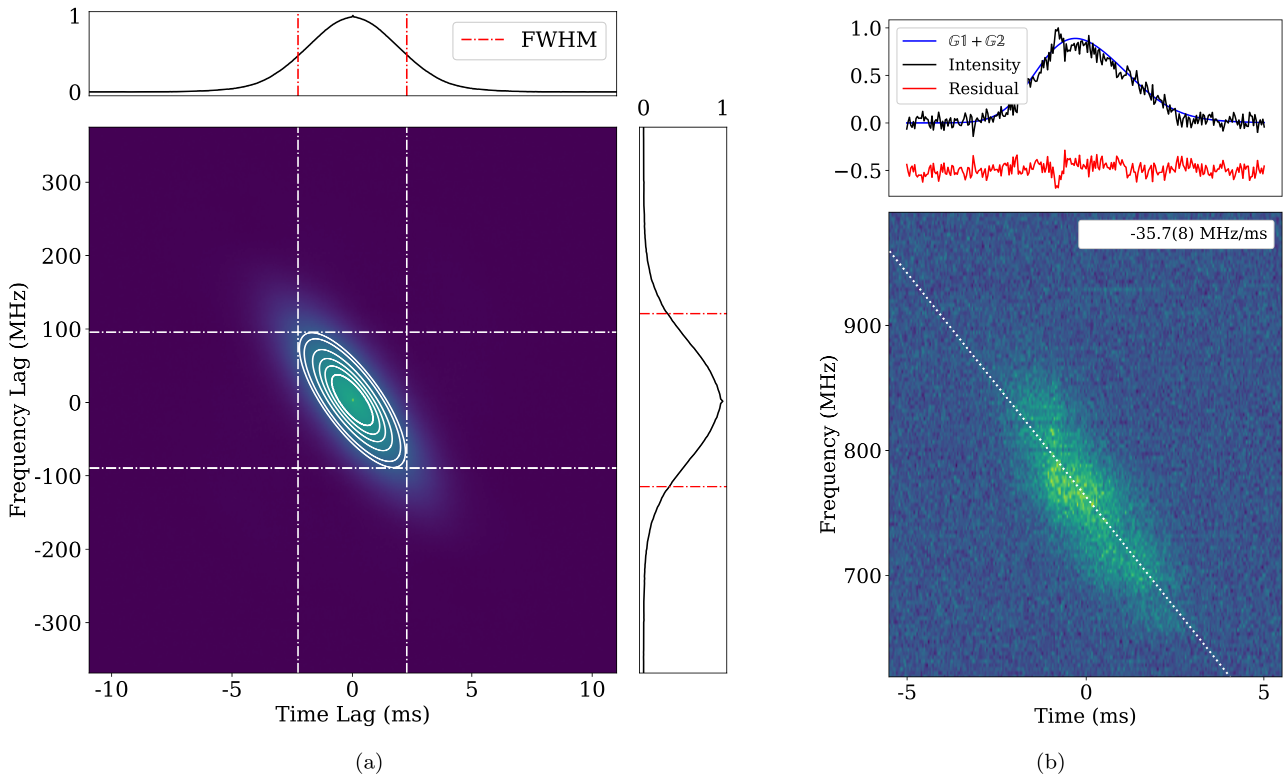

Figure 5. Drift rate estimation of burst GBT B from FRB 20180916B. (a) 2D ACF of GBT B with overlaid fitted ellipses using `photutils`. (b) Dynamic spectrum with over-plotted dashed line revealing the drift rate, as well as the burst profile with fitted double exponentially modified Gaussians.

approximately 2.94 kHz for an observing frequency of 800 MHz. For the GMRT bursts our recorded frequency resolution of 98 kHz was insufficient to observe any scintillation effect. To perform the analysis for GBT bursts, archive files were re-generated from the baseband data with frequency and time resolutions of 0.98 kHz and 1.00 ms, respectively. Using the on-pulse spectrum, we identified the centroid of each burst (the point of peak brightness) by fitting a Gaussian curve to its spectrum. We then excised 75 MHz of bandwidth centered on the centroid frequency (roughly 794 MHz for GBT B and 782 MHz for GBT E) from the dynamic spectrum, which we used to calculate an ACF. The bandwidth was cropped around the brightest part of the burst to improve S/N in the ACF. Finally, as shown in Figure 6 a stacked double Lorentizan was fit to the ACF – the first to the underlying curve of the ACF, and the second to the central peak. The FWHM of the Lorentzian fit to the central peak reveals the scintillation bandwidth. For GBT B, we calculate a scintillation bandwidth of 2.6(6) kHz for a centroid frequency of 794 MHz, whereas for GBT E, despite the burst being centered slightly lower in frequency, we measured a bandwidth of 4.2(2) kHz. The scattering estimate obtained from the average bandwidth between GBT B and GBT E is around 0.04 ms. This differs quite drastically from the scattering timescale measured from the burst profile, which leads us to believe that the exponential fall-off in intensity visible in the profile is a morphological feature rather than the product of interstellar scattering.

4. DISCUSSION

4.1. *Spectro-Temporal Properties*

Repeaters are known to have complex morphologies, FRB 20121102A is an excellent example where such structures have been observed as high as 8 GHz (Gajjar et al. 2018; Hessels et al. 2019). FRB 20180916B also exhibits this property and we too observe such structures in our bursts in both the time and frequency domain. Figure 7b shows scattering estimate for FRB 20180916B at different observing frequencies, it seems to follow a power law with an index of -4 extending from 2.7 μs estimate by Marcote et al. (2020) using the scintillation bandwidth. This bandwidth estimate is in agreement with what is expected from the NE2001 model (Cordes & Lazio 2002), hence a majority of the scattering shown by the source across all frequencies can be attributed to Milky Way galaxy suggesting minimal

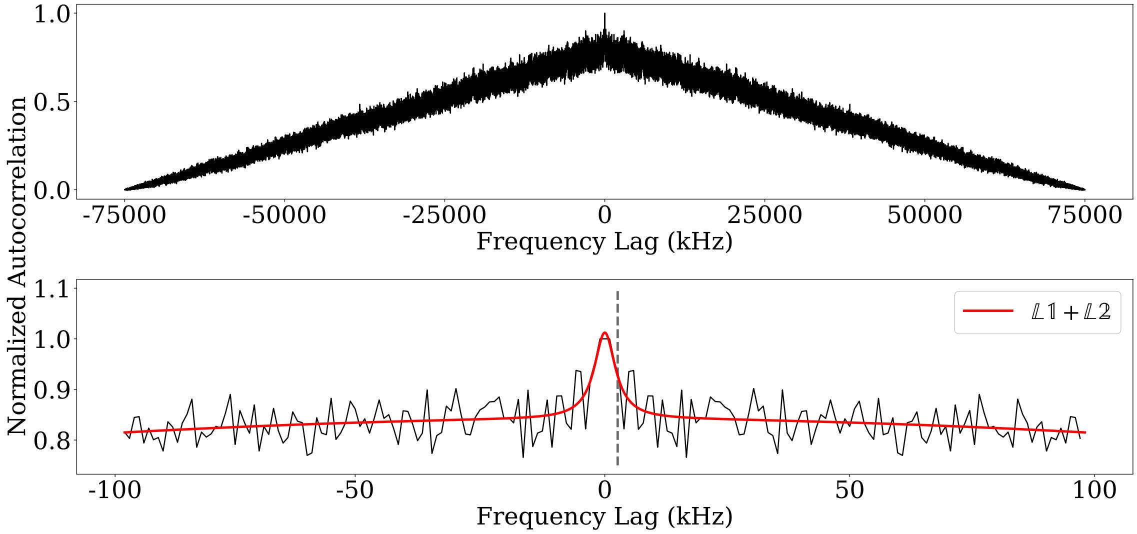

Figure 6. Scintillation bandwidth measurement for GBT B burst from FRB 20180916B. *Top:* ACF of 75 MHz of bandwidth, centered around 782 MHz (the centroid frequency). Two Lorentzian functions were fit to the central peak and broader underlying curve in the ACF. *Bottom:* The Lorentzian fit to the central peak with FWHM shown with a dotted vertical line at 2.6(6) kHz which corresponds to scintillation (decorrelation) bandwidth. This scintillation bandwidth is in agreement with the predicted bandwidth of 2.68 kHz from NE2001 (Cordes & Lazio 2002).

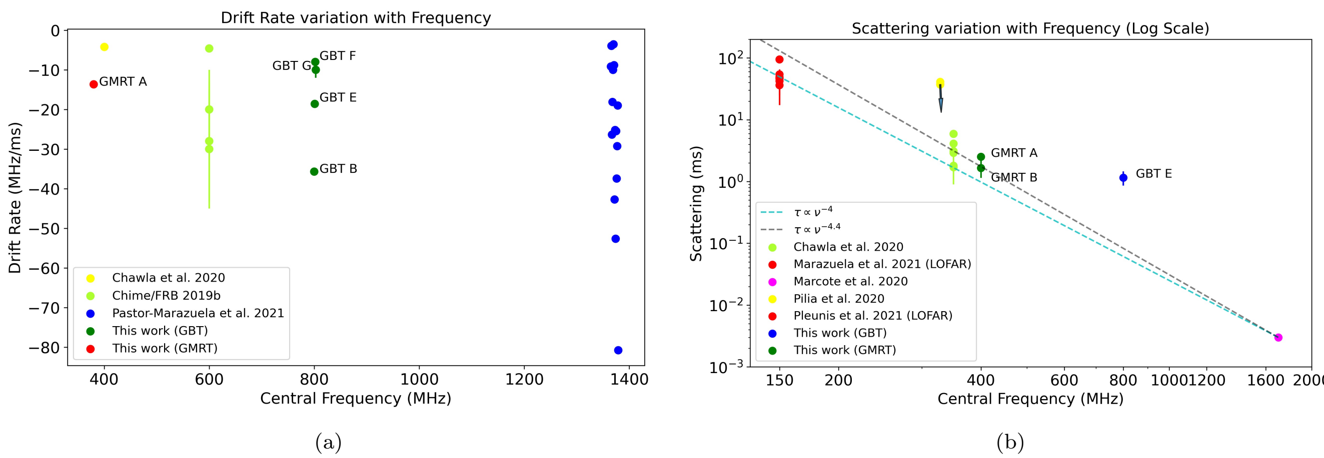

Figure 7. Comparison of drift rates and scattering as a function of observing frequencies for FRB 20180916B. (a) Measured and reported drift rates at different central frequencies. Dashed line shows a best linear fit with slope -0.02 i.e $\dot{\nu} = -0.02\nu$ indicating that the drift rate appears to increase with observing frequency. (b) Measured and reported scattering time scale as a function of observing frequencies (shown in a log scale). Assuming powerlaw of -4 or even -4.4, GMRT scattering time scales agree with expected scattering extrapolated from measured scattering time scale by Marcote et al. (2020) at a higher frequency. Variation in scattering time scale in GBT E burst can be due to unresolved sub-structure.

contribution from the host. Scattering measurement for the bursts in our dataset (Table 3) also concur with this trend. However unresolved structures in the bursts can inhibit an accurate estimation of scattering timescales leading to deviation from the expected value as seen for GBT E in Figure 7b. Probing deeper into these microstructures using a timeseries autocorrelation analysis (see Section 3.1) we found GBT F showing structure around 30 μs wide (Figure 4a). This corresponds to an emission region of $\sim$ 10 km (using light travel time), hinting at a magnetospheric origin. In FRB 20180916B, structures have been seen down to 2 μs width by Nimmo et al. (2020) at 1700 MHz. The observation of such structures at even lower frequencies (< 1 GHz) here suggest a less dense local environment not resulting in smearing and scattering of these tiny variations in the burst envelope.

Downward drifting sub bursts are a characteristic feature of repeaters. The slope of this 'sad trombone' effect seems to increase with observing frequency. Hessels et al. (2019) first identified this phenomena in FRB 20121102A bursts by comparing the drift rate estimates from bursts detected at 1.4 GHz and 6 GHz; and this trend has also been observed for FRB 20180916B by Pastor-Marazuela et al. (2021). As shown in Figure 7a, our drift rate estimate for GMRT bursts (GMRT A) and GBT bursts (GBT B and GBT E), measured in the same activity cycle of the source, does follow a linear trend with observing frequency. In Figure 7a, we applied the best fit slope, taking into consideration mean of the drift rates at particular observing frequency. Though, the large scatter in the measured drift rate (see Figure 7a) does suggest a varying rates from burst-to-burst fluctuations at similar frequencies. Frequency normalised drift rate i.e drift rate divided by observed frequency (unit will be $(\text{ms})^{-1}$) appears to be bounded by -6% from the base value (i.e no drifting). Although more data points are needed, especially in lower frequencies, to check consistency with this bound, such a possibly frequency-independent measure may be of ready guidance in assessing models explaining the drift.

Overall, this correlation study for other repeating FRBs will be fundamental in modeling the emission mechanism shown by repeaters. Recent studies have also revealed a relation between the drift rates and temporal widths of individual sub-bursts for repeating sources (Chamma et al. 2020). This was not possible to investigate for our observations as S/N of the detected bursts were not sufficient enough to identify discrete temporal sub-bursts (except GMRT A; see Figure 3). However, we were able to resolve spectral striations and able to measure scintillation bandwidth (section 3.4), which is in agreement with what is expected from Milky Way (Cordes & Lazio 2002).

4.2. *Phase-Frequency activity relation*

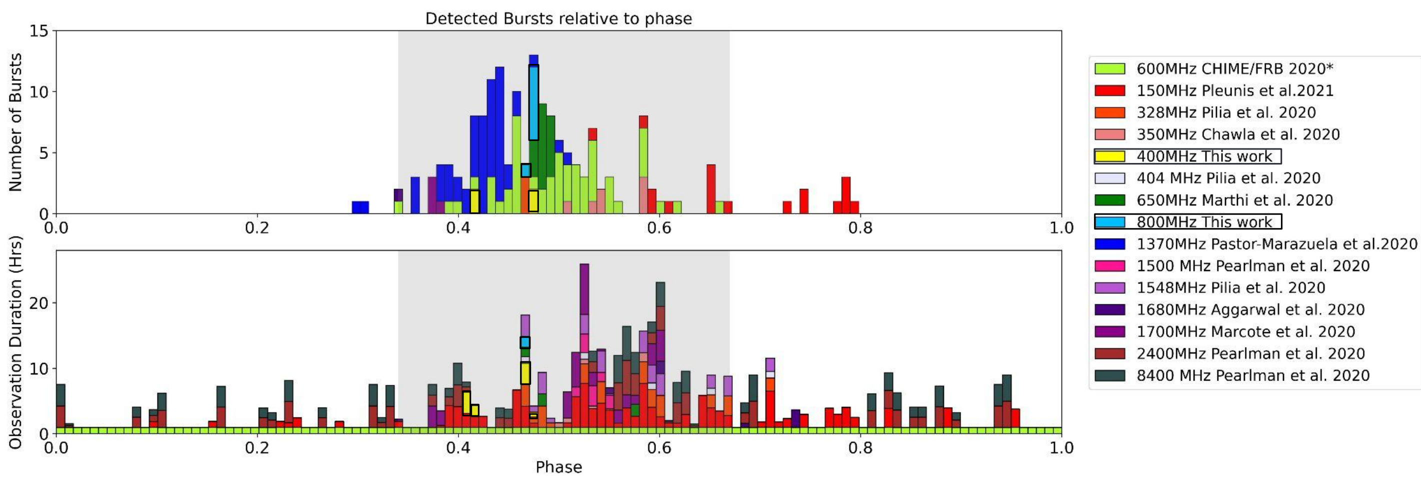

Figure 8. Frequency dependent activity window of FRB 20180916B. *Top:* Phase distribution of detected bursts with respect to frequencies folded at a period of 16.33 days with reference to MJD 58369.40 (Pleunis et al. 2021). We see a clear shift in peak activity as we move from higher to lower observing frequencies. *Bottom:* Observation hours at different phases for all observed frequencies. Here we see searches have been done beyond the activity window to constraint the periodicity, notably higher frequencies yielding no detections. We report here CHIME/FRB detections upto 20th September 2020. The gray shaded region shows the activity window.

Frequency dependence in the activity of FRB 20180916B is now well established (Aggarwal et al. 2020; Pastor-Marazuela et al. 2021; Pleunis et al. 2021). As shown in Figure 8, higher frequency detections occur earlier within the activity phase, with LOFAR detections occuring much later in the activity phase, in a few cases even beyond the predicted activity window. The grey region (0.37 - 0.64 in activity phase) was the initial estimate on the 'activity' window by CHIME/FRB (The CHIME/FRB Collaboration et al. 2020). Pastor-Marazuela et al. (2021) found that the window seems to get narrower with increment in observing frequency but they also found that burst rate can vary with cycle even during the expected 'peak' activity as was seen in their Apertif observations. Estimation of burst rate with frequency at different phases over multiple cycles will help quantitatively estimate the activity of the source in both spectral and temporal phases. Overall, on comparing the peak activity we do see a downward trend in frequency with phase, i.e. lower-frequencies appears to have later peak activity.

Our simultaneous GBT and GMRT observation epoch (0.46-0.48 in activity phase) perfectly follows this trend. We detected 7 bursts from the source in 1.67 hours of observation with GBT (800 MHz) this puts the burst rate to be $4.2^{+4.4}_{-2.5}$ bursts per hour above fluence limit of 0.9 Jy ms with 95 % confidence limit. Interestingly during this hyperactivity, there were no detections in the uGMRT band (400 MHz) but we did detect two bursts in the same observing session (see Figure 1), hence with a total of 2.85 hours of on-source time we get a burst rate of around $0.7^{+1.8}_{-0.6}$ bursts per hour above 1.6 Jy ms fluence limit in the simultaneous observing window.

The fluence limits for both telescopes correspond to a 2 ms wide bursts with S/N>10 detection assuming burst spectrum equal or smaller than our observed bandwidths. The GBT rate is 6 times that of GMRT which can be due to our observations being in the peak activity of the source at 800 MHz. This can be seen in Figure 8 as GBT bursts seem to lie between the 'peak' activity of Apertif (1370 MHz) and CHIME/FRB (600 MHz) detections. Such a high rate can also be serendipitous as such clustering of bursts in arrival times have already been seen for FRB 20121102A Gajjar et al. (2018); Zhang et al. (2018); Li et al. (2021). The more interesting aspect is the complete lack of detections at lower frequencies (400 MHz) in the simultaneous time window which might hint that the FRB remains active in one frequency range at a time. This can be due to beam geometry alignment with our line-of-sight or something intrinsic to the emission mechanism itself.

This one instance is not enough to conclusively comment on this frequency-dependent clustering but more such simultaneous observations with burst rate estimates spanning different phases will provide a more definitive picture, this is a topic for future research.

4.2.1. *Frequency Dependent Spectral Variation*

Spectrally-limited emissions have now been well associated with repeaters (The CHIME/FRB Collaboration et al. 2021a; Kumar et al. 2020). We too observe narrow emissions with varying central frequency in GMRT, GBT, and CHIME bands; although GMRT A and GMRT B cover almost the entire bandwidth. There is a lack of simultaneous emission as it is evident from Figure 2. This restricts an exact estimation of the spectral index. To understand the energy distribution and its frequency dependence, Houben et al. (2019) characterized statistical spectral index $\alpha_{\rm s}$, which takes into consideration statistical variability of the spectrum (or energy distribution) at different frequencies depending upon the frequency-dependent burst rate. The relation derived is as follows:

$$\frac{\lambda_1}{\lambda_2} = \left(\frac{\nu_1}{\nu_2}\right)^{-\alpha_{\rm s}\gamma} \left(\frac{F_{\nu_1,\rm min}}{F_{\nu_2,\rm min}}\right)^{\gamma+1}. \tag{2}$$

Here, γ is the power-law index which is taken to be $-2.3^{+0.4}_{-0.4}$ as estimated by The CHIME/FRB Collaboration et al. (2020). λ_1 and λ_2 corresponds to burst rates at central frequencies $\nu_1 = 400\,\rm MHz$ and $\nu_2 = 800\,\rm MHz$, respectively. $F_{\nu,\rm min}$ is taken to be 0.9 times the fluence of the weakest burst detected. In this case it is 1.39 Jy ms for GMRT ($0.9 \times$ GMRT C) and 0.22 Jy ms for GBT ($0.9 \times$ GBT D). After performing 10,000 simulations by randomly sampling values of λ_1, λ_2, and γ assuming Gaussian distribution using the mean and error range given above, we get $\alpha_s = -0.6^{+1.8}_{-0.9}$ with reported 95% confidence limit.

Our measured statistical spectral index for FRB 20180916B is slightly higher than what was already reported by Chawla et al. (2020), although agrees well within error bars. This slight discrepancy can be explained by an unusually high burst rate at the GBT band in just 1.67 hours of observation which can be serendipitous or point to something intrinsic about the source. Notably, our observations are also at an earlier active phase than what was reported by Chawla et al. (2020); which can be suggestive of phase-dependent energy distribution similar to phase-dependent active emission frequency as mentioned in previous section. This varying emission at different central frequencies still needs to be understood, it can possibly be something intrinsic to the emission region or a characteristic of propagation due to various phenomenon such as plasma lensing or a refractive local medium (Cordes et al. 2017). More such simultaneous observations and estimation of the statistical spectral index across the activity window will aid better constraint the distribution of burst energetics and possible emission mechanisms.

4.3. *Burst Energetics*

FRB 20180916B is one of the closest repeating FRB sources that has been localised with an accurate distance estimate. Its frequent activity makes it ideal to study the energy budget of the source across multiple wavelengths in the radio regime. With our statistical spectral index estimation in section 4.2 we found that their might be a phase-frequency dependence in energy distribution for the source, hence by comparing the energetics of individual bursts we can cumulatively estimate the energy released by the source at certain activity phase at different frequencies. Multiband observations such as this are ideal for such studies. This can help better understand the emission mechanism at play and narrow down possible progenitor scenarios responsible for these events.

Figure 9 shows the spectral energy distribution of bursts detected from FRB 20180916B at various central frequencies and also make a comparison with energies of bursts from SGR 1935+2154. The spectral energy spans 4 orders of magnitude ranging from 10^{27} to 10^{31} ergs/Hz. The source is brighter at lower frequencies; this can be attributed to detection of only the brightest of bursts due to high sky temperatures at these frequencies. However, non-detection of such highly energetic emissions at >300 MHz does put some constraint on the emission scenarios. We also detect brighter bursts at the GMRT band (400 MHz) compared to the GBT band (800 MHz), this cannot be attributed to the sensitivity of the telescopes as GMRT is capable of detecting bursts at energies around that of the weakest GBT burst i.e GBT D. Marthi et al. (2020) did observe as of yet the weakest detections from the source at 650 MHz with GMRT, observing around the same epoch as our observations. It is noteworthy though that Pearlman et al. (2020) limits emission at S-band (2.3 GHz - 0.26 Jy ms) and X-band (8.4 GHz - 0.14 Jy ms) are comparable to the weakest detections observed in our case. Hence, the lack of high-frequency emission (> 2GHz) is likely to be intrinsic to the source, meaning the source can be active but not energetic enough at a frequency range this can lead to no or very few detections at that frequency range potentially affecting the periodicity estimates.

This brings the spectral energy budget in radio wavelength within an order of magnitude of what has been observed for the FRB detected from SGR 1935+2154. It is noteworthy that this burst was detected across a wide band, which includes 1.4 GHz detection by STARE2 (Bochenek et al. 2020) and detection down to 400 MHz by CHIME/FRB (CHIME/FRB Collaboration et al. 2020) and possibly extending beyond these observing bands. This is equivalent to a bandwidth of more than 1000 MHz and taking a spectral energy estimates to be $\sim 10^{26}$ ergs/Hz the total energy amounts to 10^{32} ergs which comparable to total energy of burst from FRB 20180916B. This is due to the fact that in some cases the bandwidths of bursts from FRB 20180916B are < 50 MHz (as for GBT A in our case) which amounts to energy in similar order of magnitudes. However, we should note that this is only true if we assume the narrow bandwidth emission is intrinsic to the source. The other caveat here is large uncertainty in the distance to SGR 1935+2154 which can affect the energy argument by a few orders of magnitude. We can also see that SGR bursts will not be detected by any of our telescopes if it was at the distance of FRB 20180916B, this does put into perspective the number of weaker detections we are missing at different frequencies; which might also affect the periodicity estimate. Narrowband emissions or flux knots have now been observed in giant pulses of PSR J0540-6919 (Geyer et al. 2021) and Crab pulsar (Thulasiram & Lin 2021), which has been attributed to intrinsic emission behaviour of the source. Moreover, the discovery of FRB in a globular cluster near M81 (Bhardwaj et al. 2021; Kirsten et al. 2021; Majid et al. 2021) does put forward a strong case for the relationship between giant pulses and FRBs. Another outburst comparable to FRB luminosity from a galactic source will surely help us better constrain the energy gap between these two phenomena.

4.4. *DM and RM variations*

DM variability is a strong indicator of the changes in the local environment of the source, providing meaningful constraints on emission mechanisms as well as possible progenitor scenarios. FRB 20121102A showed a DM increase of $\sim$ 1-3 $\mathrm{pc\,cm^{-3}}$ (Hessels et al. 2019), supporting the hypothesis of source being embedded in a dense nebula (Michilli et al. 2018). No such variation has been observed in the case of FRB 20180916B since its detection by CHIME/FRB. The initial estimated value of 348.82 $\mathrm{pc\,cm^{-3}}$ (The CHIME/FRB Collaboration et al. 2020) has been reproduced throughout in subsequent detections, with Nimmo et al. (2020) providing strongest constraint of 348.772 ± 0.006 $\mathrm{pc\,cm^{-3}}$ using microsecond time resolution. Our brightest detection GBT E has a structure maximising DM of 348.9 $\pm$ 0.1 $\mathrm{pc\,cm^{-3}}$, which is in agreement with the reported value. On inspection by eye, the dynamic spectra of all the strong drifting bursts in our dataset namely GMRT A, GBT B, GBT E and GBT F showed maximum structures around 348.8 $\mathrm{pc\,cm^{-3}}$. Other bursts seem to be weak or too fuzzy to accurately estimate their structure maximising DM. Thus, we can constraint DM variation to be < 1 $\mathrm{pc\,cm^{-3}}$. We also did not observe any DM evolution between 2 GMRT epochs. This disfavors binary wind models and also supports a cleaner environment in the case of FRB 20180916B (Pastor-Marazuela et al. 2021).

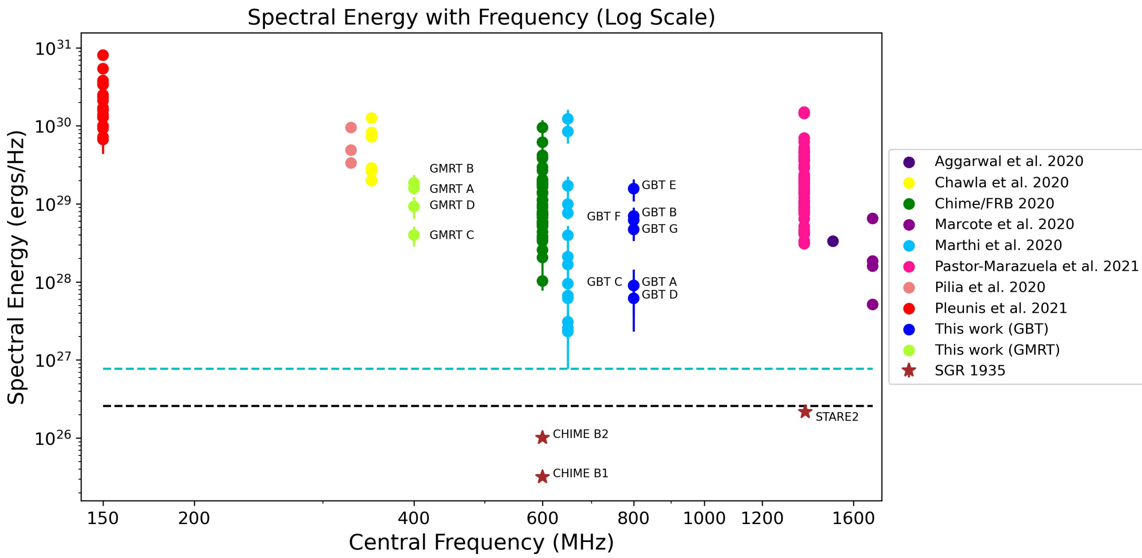

Figure 9. The spectral energy-density of bursts as a function of observing frequencies for FRB 20180916B. We see bursts at lower frequencies are brighter due to higher sky temperature permitting only the strongest detections. Although its interesting to see lack of energetic detections at > 300 MHz. We see the weakest detections from FRB 20180916B are within an order of magnitude to the spectral energy of SGR J1935+2154 (shown by dotted lines) although maximum possible distance to the source has been taken to estimate the energy (11 kpc). The distance to FRB 20190916B is taken to be 149 Mpc (Marcote et al. 2020).

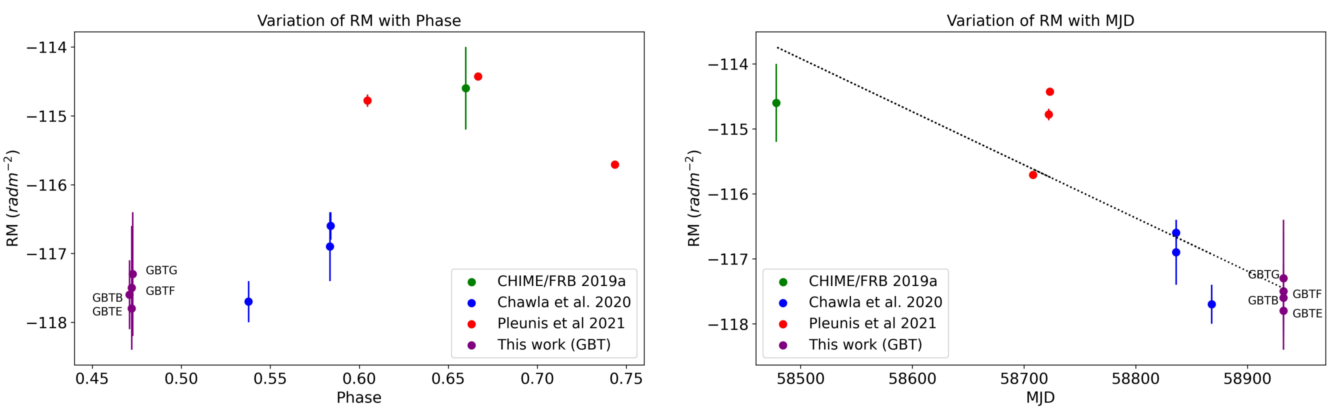

(a)

(b)

Figure 10. RM comparison for FRB 20180916B across multiple epochs and activity phases. (a) Folding the RM values as a function of activity phase for all observed epochs. Data is insufficient to observe any correlation in RM with phase, more observations in future might help uncover any underlying trend. (b) Observed RM as function of observing epoch. The RM of the source gradually decreases since the first measurement by The CHIME/FRB Collaboration et al. (2019) nearly 2 years ago. Our RM values (around $-117.5\,\mathrm{rad\,m^{-2}}$) are a unit less than the one reported by Chawla et al. (2020) for their November 2019 epoch ($-116.6\,\mathrm{rad\,m^{-2}}$) detections but similar to the one reported for their January 2020 detections ($-117.7\,\mathrm{rad\,m^{-2}}$).

We report polarisation properties of bursts detected from observations with the GBT. As shown in Figure 3 all bursts are 100% linearly polarised with no circular polarisation. The PPA is approximately flat for each burst and following calibration, we do not observe any considerable variability in PPA offsets (see Table 3). This constant flat PPA is similar to what has been observed for FRB 20121102A (Hessels et al. 2019); however, the RM values between the two sources differ by 4 orders of magnitude (Michilli et al. 2018; The CHIME/FRB Collaboration et al. 2019). Also unlike FRB 20121102A which shows a prominent decreasing trend in its RM with time (Hilmarsson et al. 2021), the RM changes slowly for FRB 20180916B. As seen in Figure 10 the RM has decreased over the two years ($\delta \sim$ 2-3 rad

m^{-2}). This change can be due to alterations in the plasma environment or electron density in the local environment but seeing the homogeneity in the DM, variations in viewing geometry can better explain this difference. We cannot comment on short time scale variability (over a month) in RM values due to lack of data, but it is certainly an interesting avenue to explore with a dedicated observing campaign. It is possible that similar to burst activity, RM might also have phase relation, however, we do not see a clear phase dependence (see Figure 10). More observations around different phases within the same activity window can uncover any likely dependence. Moreover, any variations in RM over short timescales (and phase) has to be removed to probe true nature of RM variation over longer timescales . This is difficult to do with the limited sample but may be pursued in the future.

4.5. *Progenitor models*

Numerous models have been put forward to explain the unique periodicity seen in FRB 20180916B. The prominent being a pulsar/magnetar with a binary companion (Zhang & Gao 2020; Popov 2020) which can be an O/B star (Ioka & Zhang 2020; Lyutikov et al. 2020). In such scenario, wind from the companion obscures the FRB source for most of the orbit; such scenario also favours frequency-dependent activity with wider activity window at higher frequencies. We see more activity in the GBT band (800 MHz) in comparison to GMRT band (400 MHz) during our semi-simultaneous observations. This early phase activity at higher frequencies have also been observed by Pastor-Marazuela et al. (2021). Although, they have shown a narrower activity window at higher frequencies, which disfavors such binary wind models. In addition to this, we also did not observe any DM evolution in our observations during the two GMRT observing sessions, challenging another prediction made by wind models.

Models supporting a precessing neutron star or magnetar have also tried to explain this periodicity (Levin et al. 2020; Tong et al. 2020). This framework requires a young magnetar surrounded with dense plasma; however, recent LOFAR detections (Pleunis et al. 2021; Pastor-Marazuela et al. 2021) and our energetic detections at GMRT band (400 MHz) alongwith observation of microstructures (figure 4) at GBT band (800 MHz) favour a cleaner environment. Tendulkar et al. (2020) have also challenged many claims by these models with a high-resolution study of FRB 20180916B proximity using Hubble Space Telescope. They instead favour a model involving High Mass X-ray Binary (HMXB) or a gamma-ray binary with a late O-type or B-type companion. Another interesting scenario that has tried to explain this periodicity of the source and infact its frequency dependence involves emission of FRBs in Ultra Luminous X-Ray Binaries (ULXBs) (Sridhar et al. 2021) via synchroton maser mechanism. But this model fails to explain the microsecond structures observed at different observing frequencies as seen by Nimmo et al. (2020) at 1700 MHz and in our GBT observations at 800 MHz (see Figure 4). In summary, our low-frequency detections and constant PPA (see Section 3.3) are less likely to support a young magnetar scenario inside dense environment.

5. CONCLUSION

We detected 12 bursts (4, 1 and 7) from FRB 20180916B in our 700 MHz wide observation using uGMRT (300-500 MHz), CHIME (400-800MHz) and GBT (600-1000 MHz); spread across 0.1 phase in the activity window. This includes simultaneous observation of the source by GBT and uGMRT. Our reported first detections of the source in 800-1000 MHz range indicates prolific activity of the source across 110 MHz to 1700 MHz. Since our observations were earlier than the estimated peak activity (i.e phase 0.5) we find the source to be more active in the GBT band compared to the GMRT band; which further strengths earlier indication of frequency-dependent activity window. Our estimates on the statistical spectral index also hint at the source being more energetic at higher frequencies earlier in its activity cycle. The observation of microstructure below 1 GHz here also provides evidence of a magnetospheric origin and a clean environment that doesn't lead to scattering and dissipation of these high time resolution variations in the burst envelope. The scattering seems to agree with what we can expect from our Milky Way although unresolved substructures do induce uncertainties in our estimates. The drift rate seems to increase with frequency similar to what has been observed for FRB 20121102A . We also report first polarimateric observations at 800 MHz; which is consistent with previous studies as we observe 100% linear polarization and a flat PPA. We do find that the source RM has decreased over time, although not as significant as FRB 20121102A , which is likely due to four orders of magnitude difference between the initial RM between these two sources. We do not find any significant DM variation and constraint Δ DM ~ 1 pc cm^{-3}. With our results, we disfavour the binary wind model as well as a precessing magnetar but we have a limited phase coverage to make any significant assertion. Our results show that multiband studies of repeaters or even one-off FRBs is the ideal approach to disentangle any frequency dependence in properties and activity of the source. Dedicated multi-wavelength studies of FRB 20180916B across the entire activity window, is an exciting avenue for future research.

ACKNOWLEDGMENTS

We thank Avinash Deshpande, Wael Farah, Akshay Suresh and Gaurav Waratkar for their helpful insights. We thank the staff of the GMRT that made the uGMRT observations possible. The GMRT is run by the National Centre for Radio Astrophysics of the Tata Institute of Fundamental Research.

We acknowledge that CHIME is located on the traditional, ancestral, and unceded territory of the Syilx/Okanagan people. We thank the Dominion Radio Astrophysical Observatory, operated by the National Research Council Canada, for gracious hospitality and expertise. CHIME is funded by a grant from the Canada Foundation for Innovation (CFI) 2012 Leading Edge Fund (Project 31170) and by contributions from the provinces of British Columbia, Québec and Ontario. The CHIME/FRB Project is funded by a grant from the CFI 2015 Innovation Fund (Project 33213) and by contributions from the provinces of British Columbia and Québec, and by the Dunlap Institute for Astronomy and Astrophysics at the University of Toronto. Additional support was provided by the Canadian Institute for Advanced Research (CIFAR), McGill University and the McGill Space Institute via the Trottier Family Foundation, and the University of British Columbia.

Breakthrough Listen is managed by the Breakthrough Initiatives, sponsored by the Breakthrough Prize Foundation (breakthroughinitiatives.org). The Green Bank Observatory is a facility of the National Science Foundation operated under cooperative agreement by Associated Universities, Inc.

J. Faber was generously supported by the National Science Foundation under the Berkeley SETI Research Center REU Site Grant No. 1950897. A.B.P. is a McGill Space Institute (MSI) Fellow and a Fonds de Recherche du Quebec – Nature et Technologies (FRQNT) postdoctoral fellow. E.P. acknowledges funding from an NWO Veni Fellowship.

Facilities: GMRT, GBT, CHIME

Software: `astropy` (Astropy Collaboration et al. 2013), `DM Phase` (Seymour et al. 2019), `DSPSR` (van Straten & Bailes 2011) `Gptool` (Susobhanan et al. 2020), `Heimdall` (Barsdell et al. 2012), `ionFR` (Sotomayor-Beltran et al. 2013), `Matplotlib`(Hunter 2007), `Numpy` (Harris et al. 2020), `PRESTO` (Ransom 2011), `PSRCHIVE` (Hotan et al. 2004; van Straten et al. 2011), `Scipy` (Virtanen et al. 2020), `SIGPROC` (Lorimer 2011), `SPANDAK` (Gajjar et al. 2018)

REFERENCES

Aggarwal, K., Law, C. J., Burke-Spolaor, S., et al. 2020, Research Notes of the AAS, 4, 94

Astropy Collaboration, Robitaille, T. P., Tollerud, E. J., et al. 2013, A&A, 558, A33, doi: 10.1051/0004-6361/201322068

Barsdell, B. R., Bailes, M., Barnes, D. G., & Fluke, C. J. 2012, MNRAS, 422, 379, doi: 10.1111/j.1365-2966.2012.20622.x

Beloborodov, A. M. 2017, ApJL, 843, L26, doi: 10.3847/2041-8213/aa78f3

Bhardwaj, M., Gaensler, B. M., Kaspi, V. M., et al. 2021, The Astrophysical Journal Letters, 910, L18, doi: 10.3847/2041-8213/abeaa6

Bochenek, C. D., Ravi, V., Belov, K. V., et al. 2020, Nature, 587, 59

Chamma, M. A., Rajabi, F., Wyenberg, C. M., Mathews, A., & Houde, M. 2020, arXiv e-prints, arXiv:2010.14041. https://arxiv.org/abs/2010.14041

Chatterjee, S. 2020, Progress in Understanding the Enigmatic Fast Radio Bursts. https://arxiv.org/abs/2012.10377

Chawla, P., Andersen, B., Bhardwaj, M., et al. 2020, The Astrophysical Journal Letters, 896, L41

CHIME/FRB Collaboration, Amiri, M., Bandura, K., et al. 2018, ApJ, 863, 48, doi: 10.3847/1538-4357/aad188

—. 2019, Nature, 566, 230, doi: 10.1038/s41586-018-0867-7

CHIME/FRB Collaboration, Andersen, B., Bandura, K., et al. 2020, arXiv preprint arXiv:2005.10324

Cordes, J. M., & Chatterjee, S. 2019, Annual Review of Astronomy and Astrophysics, 57

Cordes, J. M., & Lazio, T. J. W. 2002, ArXiv Astrophysics e-prints

Cordes, J. M., Wasserman, I., Hessels, J. W. T., et al. 2017, ApJ, 842, 35, doi: 10.3847/1538-4357/aa74da

Desvignes, G., Eatough, R. P., Pen, U. L., et al. 2018, The Astrophysical Journal, 852, L12, doi: 10.3847/2041-8213/aaa2f8

Fonseca, E., Andersen, B. C., Bhardwaj, M., et al. 2020, arXiv e-prints, arXiv:2001.03595. https://arxiv.org/abs/2001.03595

Gajjar, V., Siemion, A. P. V., Price, D. C., et al. 2018, ApJ, 863, 2, doi: 10.3847/1538-4357/aad005

Gajjar, V., Siemion, A., Croft, S., et al. 2019, in BAAS, Vol. 51, 223. https://arxiv.org/abs/1907.05519

Geyer, M., Serylak, M., Abbate, F., et al. 2021, Monthly Notices of the Royal Astronomical Society, 505, 4468–4482, doi: 10.1093/mnras/stab1501

Gourdji, K., Michilli, D., Spitler, L., et al. 2019, The Astrophysical Journal Letters, 877, L19

Harris, C. R., Millman, K. J., van der Walt, S. J., et al. 2020, Nature, 585, 357–362, doi: 10.1038/s41586-020-2649-2

Haslam, C., Salter, C., Stoffel, H., & Wilson, W. 1982, Astronomy and Astrophysics Supplement Series, 47, 1

Hessels, J. W. T., Spitler, L. G., Seymour, A. D., et al. 2019, ApJL, 876, L23, doi: 10.3847/2041-8213/ab13ae

Hilmarsson, G. H., Michilli, D., Spitler, L. G., et al. 2021, The Astrophysical Journal, 908, L10, doi: 10.3847/2041-8213/abdec0

Hotan, A., Van Straten, W., & Manchester, R. 2004, Publications of the Astronomical Society of Australia, 21, 302

Houben, L. J. M., Spitler, L. G., ter Veen, S., et al. 2019, Astronomy & Astrophysics, 623, A42, doi: 10.1051/0004-6361/201833875

Hunter, J. D. 2007, Computing in Science Engineering, 9, 90, doi: 10.1109/MCSE.2007.55

Ioka, K., & Zhang, B. 2020, The Astrophysical Journal Letters, 893, L26

Isaacson, H., Siemion, A. P., Marcy, G. W., et al. 2017, Publications of the Astronomical Society of the Pacific, 129, 054501

Kirsten, F., Marcote, B., Nimmo, K., et al. 2021, A repeating fast radio burst source in a globular cluster. https://arxiv.org/abs/2105.11445

Kumar, P., Shannon, R. M., Flynn, C., et al. 2020, Monthly Notices of the Royal Astronomical Society, 500, 2525–2531, doi: 10.1093/mnras/staa3436

Law, C. J., Abruzzo, M. W., Bassa, C. G., et al. 2017, ArXiv e-prints. https://arxiv.org/abs/1705.07553

Lebofsky, M., Croft, S., Siemion, A. P., et al. 2019, Publications of the Astronomical Society of the Pacific, 131, 124505

Levin, Y., Beloborodov, A. M., & Bransgrove, A. 2020, The Astrophysical Journal Letters, 895, L30

Li, D., Wang, P., Zhu, W. W., et al. 2021, arXiv e-prints, arXiv:2107.08205. https://arxiv.org/abs/2107.08205

Lorimer, D. R. 2011, SIGPROC: Pulsar Signal Processing Programs. http://ascl.net/1107.016

Lorimer, D. R., & Kramer, M. 2004, Handbook of Pulsar Astronomy, Vol. 4

Lyutikov, M., Barkov, M. V., & Giannios, D. 2020, The Astrophysical Journal Letters, 893, L39

MacMahon, D. H. E., Price, D. C., Lebofsky, M., et al. 2018, Publications of the Astronomical Society of the Pacific, 130, 044502, doi: 10.1088/1538-3873/aa80d2

Majid, W. A., Pearlman, A. B., Prince, T. A., et al. 2021, Astrophys. J. Lett., 919, L6, doi: 10.3847/2041-8213/ac1921

Marcote, B., Nimmo, K., Hessels, J. W. T., et al. 2020, Nature, 577, 190, doi: 10.1038/s41586-019-1866-z

Marthi, V. R., Gautam, T., Li, D., et al. 2020, arXiv e-prints, arXiv:2007.14404. https://arxiv.org/abs/2007.14404

Metzger, B. D., Margalit, B., & Sironi, L. 2019, Monthly Notices of the Royal Astronomical Society, 485, 4091–4106, doi: 10.1093/mnras/stz700

Michilli, D., Seymour, A., Hessels, J. W. T., et al. 2018, Nature, 553, 182, doi: 10.1038/nature25149

Nimmo, K., Hessels, J. W. T., Keimpema, A., et al. 2020, Microsecond polarimetry of the repeating FRB 20180916B. https://arxiv.org/abs/2010.05800

Pastor-Marazuela, I., Connor, L., van Leeuwen, J., et al. 2021, Nature, 596, 505

Pearlman, A. B., Majid, W. A., Prince, T. A., et al. 2020, arXiv preprint arXiv:2009.13559

Petroff, E., Hessels, J. W. T., & Lorimer, D. R. 2021, Fast radio bursts at the dawn of the 2020s. https://arxiv.org/abs/2107.10113

Pilia, M., Burgay, M., Possenti, A., et al. 2020, arXiv preprint arXiv:2003.12748

Pleunis, Z., Michilli, D., Bassa, C. G., et al. 2021, The Astrophysical Journal Letters, 911, L3, doi: 10.3847/2041-8213/abec72

Popov, S. B. 2020, Research Notes of the AAS, 4, 98

Ransom, S. 2011, PRESTO: PulsaR Exploration and Search TOolkit. http://ascl.net/1107.017

Reddy, S. H., Kudale, S., Gokhale, U., et al. 2017, Journal of Astronomical Instrumentation, 6, 1641011

Remazeilles, M., Dickinson, C., Banday, A., Bigot-Sazy, M.-A., & Ghosh, T. 2015, Monthly Notices of the Royal Astronomical Society, 451, 4311

Sand, K. R., Gajjar, V., Pilia, M., et al. 2020, The Astronomer's Telegram, 13781, 1

Seymour, A., Michilli, D., & Pleunis, Z. 2019, DM_phase: Algorithm for correcting dispersion of radio signals. http://ascl.net/1910.004

Sotomayor-Beltran, C., Sobey, C., Hessels, J. W. T., et al. 2013, A&A, 552, A58, doi: 10.1051/0004-6361/201220728

Spitler, L. G., Cordes, J. M., Hessels, J. W. T., et al. 2014, ApJ, 790, 101, doi: 10.1088/0004-637X/790/2/101

Sridhar, N., Metzger, B. D., Beniamini, P., et al. 2021, Periodic Fast Radio Bursts from Luminous X-ray Binaries. https://arxiv.org/abs/2102.06138

Susobhanan, A., Maan, Y., Joshi, B. C., et al. 2020, pinta: The uGMRT Data Processing Pipeline for the Indian Pulsar Timing Array. https://arxiv.org/abs/2007.02930

Tendulkar, S. P., de Paz, A. G., Kirichenko, A. Y., et al. 2020, The 60-pc Environment of FRB 20180916B. https://arxiv.org/abs/2011.03257

The CHIME/FRB Collaboration, :, Andersen, B. C., et al. 2019, arXiv e-prints, arXiv:1908.03507. https://arxiv.org/abs/1908.03507

The CHIME/FRB Collaboration, Amiri, M., Andersen, B. C., et al. 2020, arXiv e-prints, arXiv:2001.10275. https://arxiv.org/abs/2001.10275

The CHIME/FRB Collaboration, Amiri, M., Andersen, B. C., et al. 2021a, The First CHIME/FRB Fast Radio Burst Catalog. https://arxiv.org/abs/2106.04352

The CHIME/FRB Collaboration, :, Amiri, M., et al. 2021b, arXiv e-prints, arXiv:2106.04352. https://arxiv.org/abs/2106.04352

Thulasiram, P., & Lin, H.-H. 2021, Narrow-banded giant pulses from the Crab pulsar. https://arxiv.org/abs/2105.13316

Tong, H., Wang, W., & Wang, H.-G. 2020, arXiv preprint arXiv:2002.10265

van Straten, W., & Bailes, M. 2011, Publications of the Astronomical Society of Australia, 28, 1–14, doi: 10.1071/as10021

van Straten, W., Demorest, P., Khoo, J., et al. 2011, PSRCHIVE: Development Library for the Analysis of Pulsar Astronomical Data. http://ascl.net/1105.014

Virtanen, P., Gommers, R., Oliphant, T. E., et al. 2020, Nature Methods, 17, 261–272, doi: 10.1038/s41592-019-0686-2

Worden, S. P., Drew, J., Siemion, A., et al. 2017, Acta Astronautica, 139, 98

Zhang, X., & Gao, H. 2020, Monthly Notices of the Royal Astronomical Society: Letters, 498, L1

Zhang, Y. G., Gajjar, V., Foster, G., et al. 2018, ApJ, 866, 149, doi: 10.3847/1538-4357/aadf31